Supporting Information

Multifunctional amine mediated COF nanosheets for desalination membrane

Junyi Zhao, Mengqi Bie, Qian Sun, Ziting Zhu, Sui Zhang*, Fusheng Pan* and Zhongyi Jiang*

*Correspondence author. Email: chezhangsui@nus.edu.sg fspan@tju.edu.cn and zhyjiang@tju.edu.cn

This PDF file includes:

1. Supplementary methods

SEM images were carried out by a Regulus 8100 instrument. TEM, HR-TEM, and electron diffraction were examined by JEOL JEM-F200 electron microscope. XRD curves were collected by a Smartlab instrument with Cu Kα radiation. AFM images were acquired on Bruker Dimension Icon atomic force microscopy. The GIWAXS data were obtained at 1W1A Diffuse X-ray Scattering Station, Beijing Synchrotron Radiation Facility (BSRF-1W1A). Zeta potentials were taken from a Nano ZS instrument with a 4 mW He-Ne laser. FT-IR patterns were taken from Thermo Scientific Nicolet iS50. XPS was performed on an ESCALAB Xi+ instrument with an Al Kα radiation source. WACs were measured by POWEREACH JC2000D2M static contact angle goniometer. The water states in COF nanochannels were investigated by DSC (Germany's Netzsch, 200 F3). Quartz crystal microbalance (QCM, Q-sense E1, Biolin Scientific) was used to record the water-capture ability which was calculated by the modified Sauerbrey Equation (1):

$$\Delta m = -\Delta f \frac{\sqrt{\rho_q \mu_q}}{2 f_0^2} \quad (1)$$

Where Δm is the mass change on the sensor surface (μg cm^{-2}); Δf is the frequency change (Hz); f0 is the resonant frequency of the sensor (Hz); ρq and μq are intrinsic parameters of quartz crystal: density (μg cm^{-3}) and shear modulus (μg cm^{-1} s^{-2}).

2. Supplementary Figures

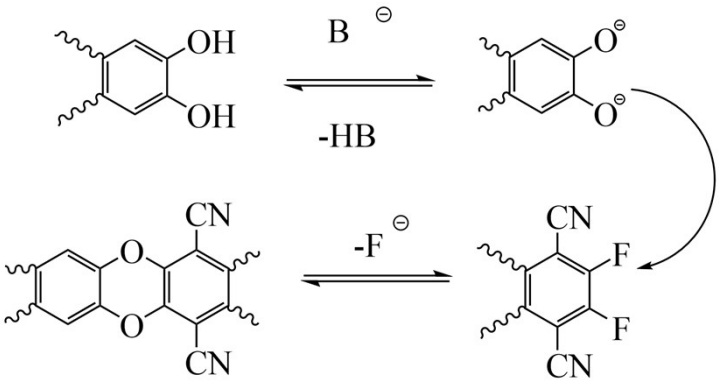

Figure S1. Proposed mechanism of dioxin linkage formation catalyzed by traditional catalyst.

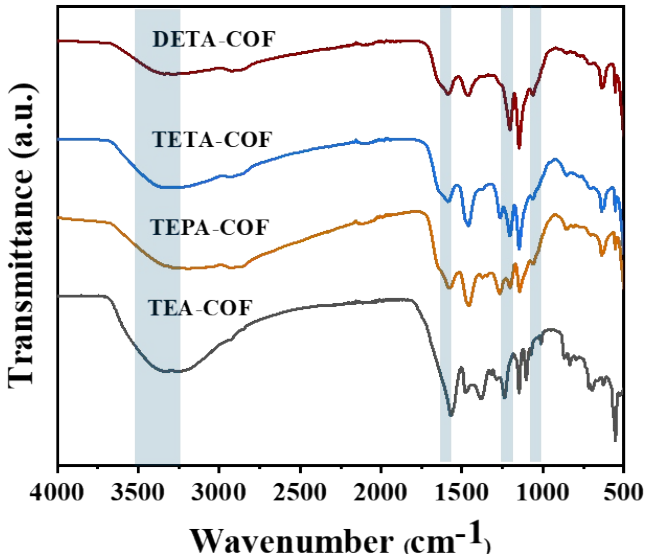

Figure S2. FT-IR spectra of DETA-COF, TETA-COF, TEPA-COF, and TEA-COF. Noted that compared with TEA-COF, both DETA-COF, TETA-COF, and TEPA-COF exhibit new peaks at 1620 cm^{-1} attributed to C=N.

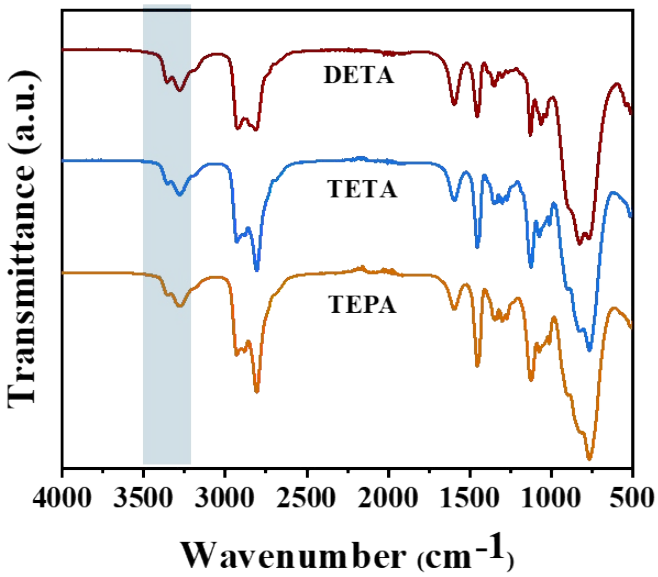

Figure S3. FT-IR spectra of DETA, TETA, and TEPA monomer.

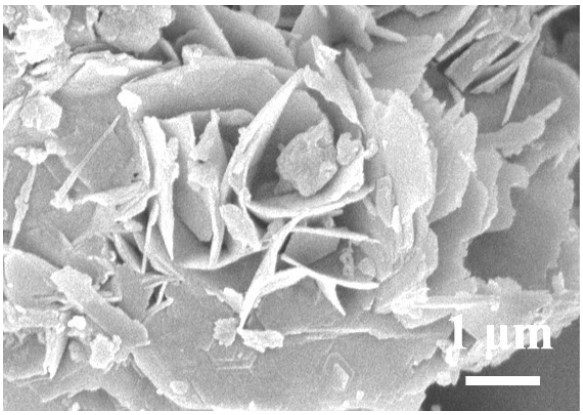

Figure S4. SEM images TETA-COF nanosheets.

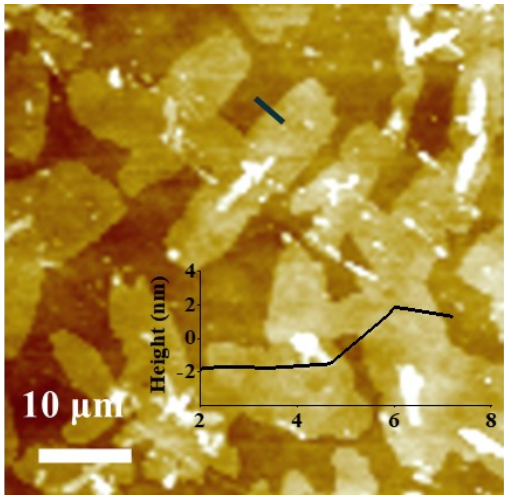

Figure S5. AFM images of TETA-COF nanosheets and the respective height profiles along the marked black line.

Figure S6. Tyndal effect of TETA-COF nanosheets aqueous dispersion.

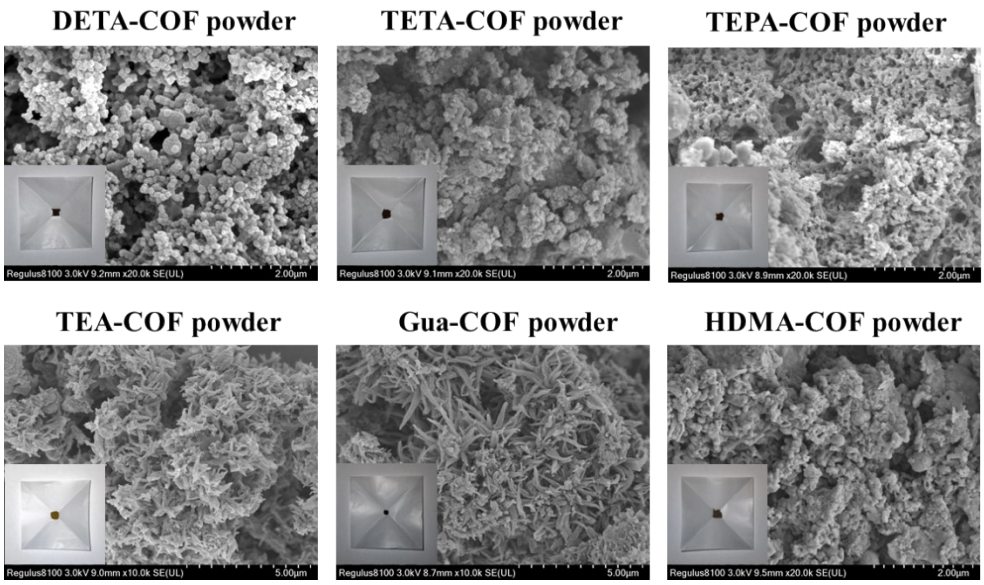

Figure S7. Photographic images and corresponding SEM images of the X-COF powders synthesized from the solvothermal method.

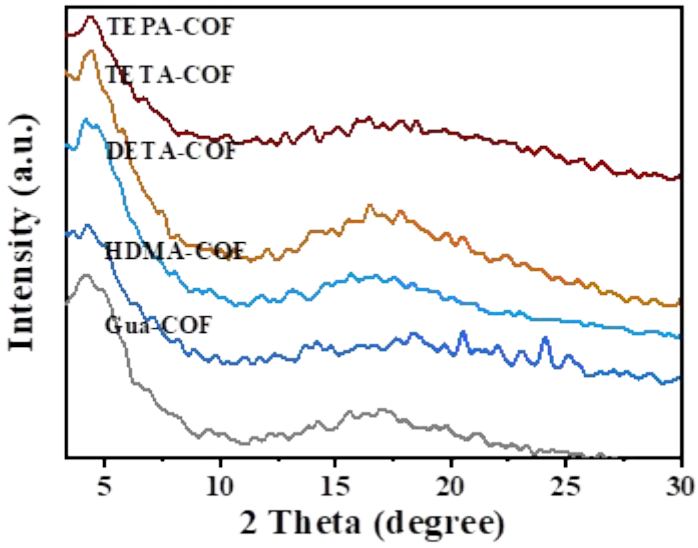

Figure S8. PXRD patterns of X-COF bulk powders synthesized by solvothermal synthesis.

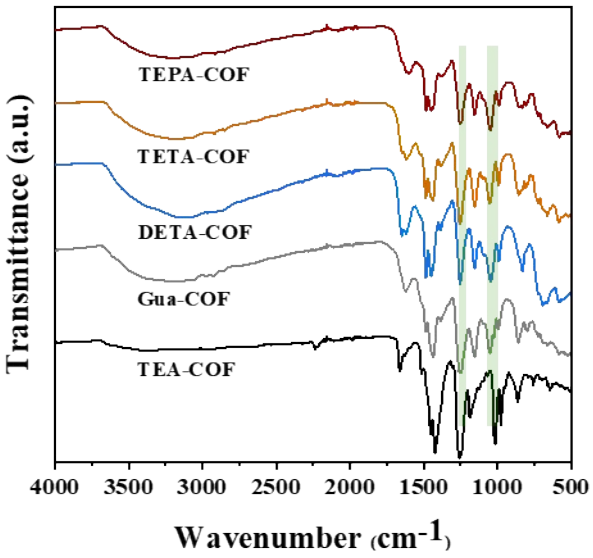

Figure S9. FT-IR spectra of X-COF powders synthesized by solvothermal synthesis.

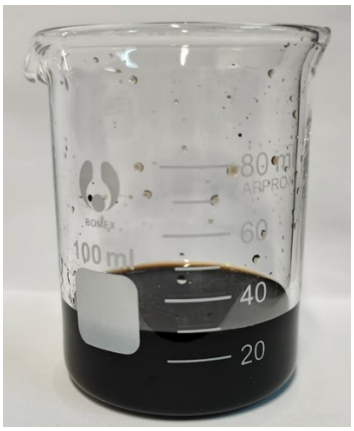

Figure S10. Photographic image of the suspension of oligomers dissolved in DMF.

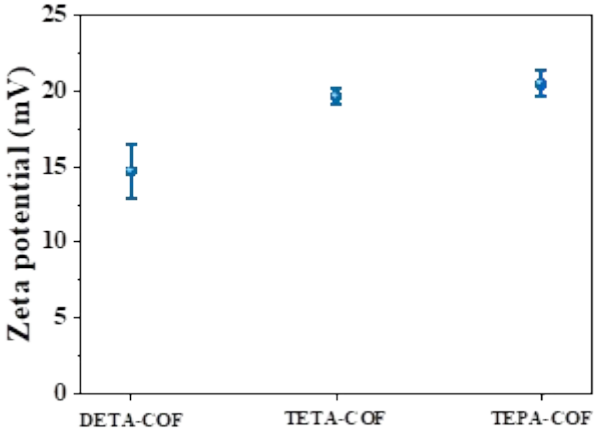

Figure S11. Zeta potential of DETA-COF, TETA-COF, and TEPA-COF nanosheet aqueous dispersion.

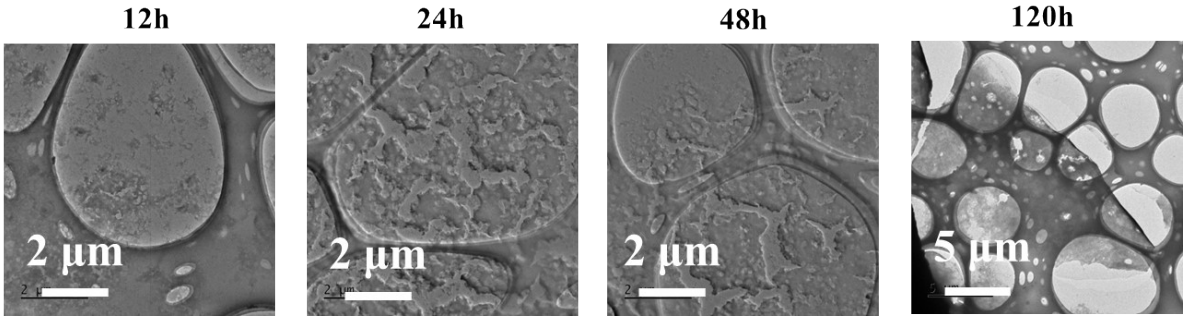

Figure S12. Time-dependent TEM images during the formation of TETA-COF nanosheets.

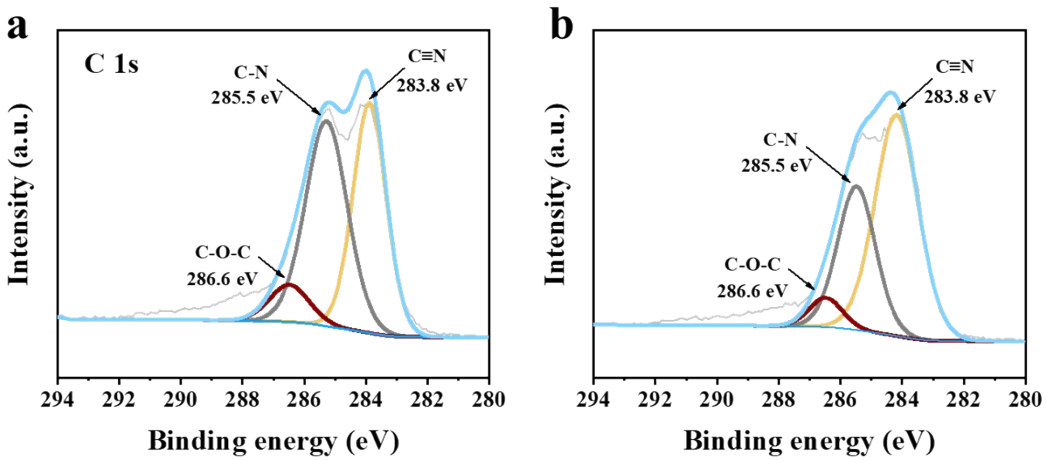

Figure S13. High-resolution XPS spectra of deconvoluted C 1s of heterogenous a) DETA-COF and b) TEPA-COF.

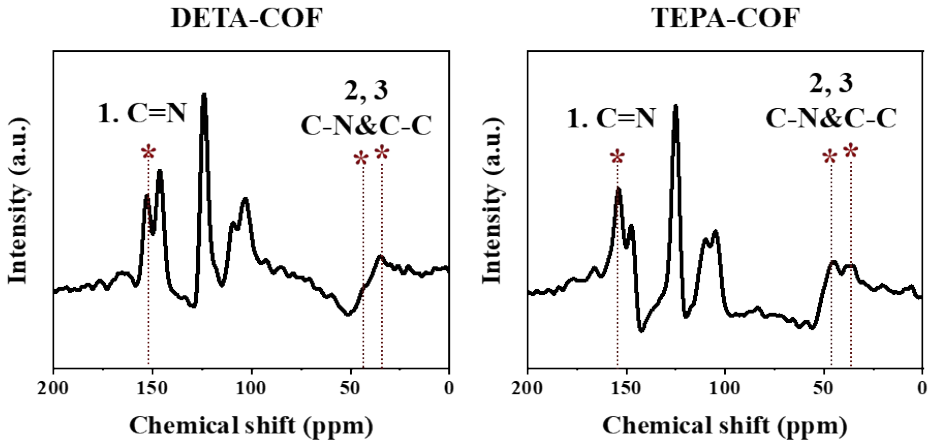

Figure S14. Solid-state 13C NMR spectrum of DETA-COF and TEPA-COF.

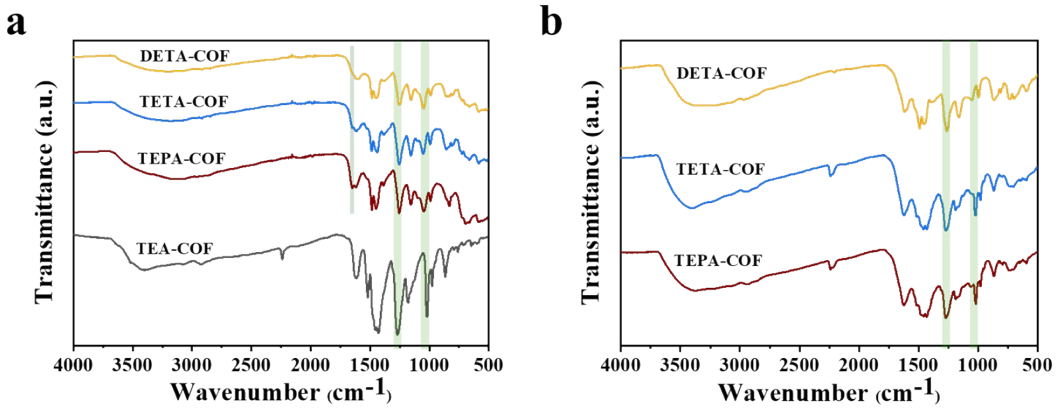

Figure S15. FT-IR spectra of the TETA-COF, DETA-COF, and TEPA-COF (a) before and (b) after the TFPN replacement.

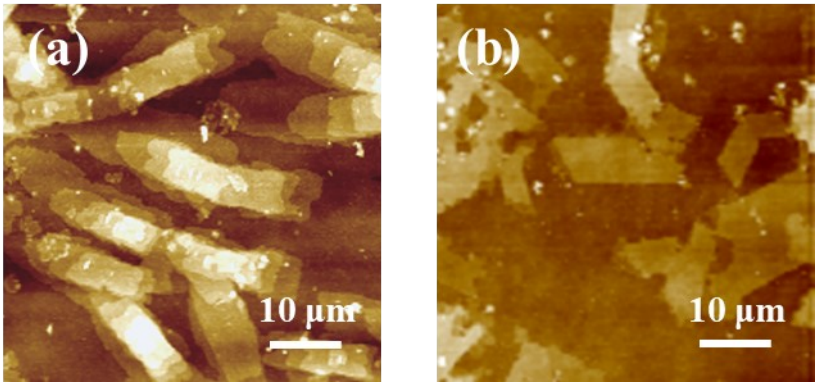

Figure S16. AFM images of the first type of amine catalyst. a) DETA-COF nanosheets. b) TEPA-COF nanosheets.

Figure S17. Comparison of Tyndall effect of TEA-COF, DETA-COF, TETA-COF, and TEPA-COF nanosheets aqueous dispersion. The great Tyndall effect indicates processability.

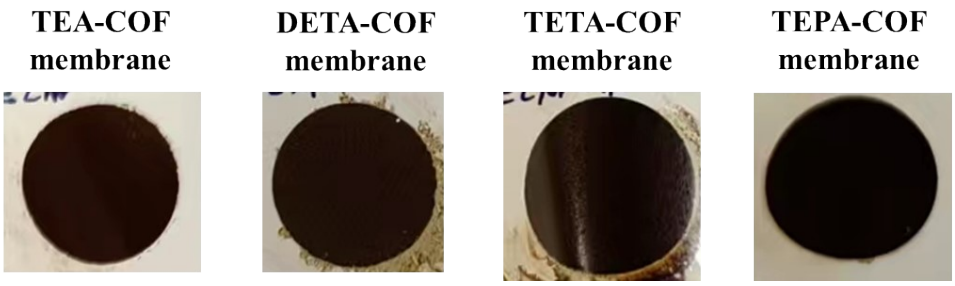

Figure S18. Photograph of various types of X-COF membranes.

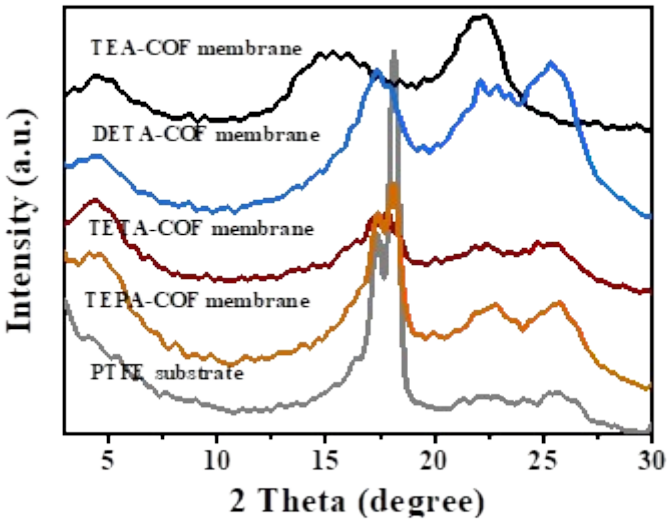

Figure S19. XRD patterns of the DETA-COF, TETA-COF, TEPA-COF, TEA-COF membranes, and PTFE substrate.

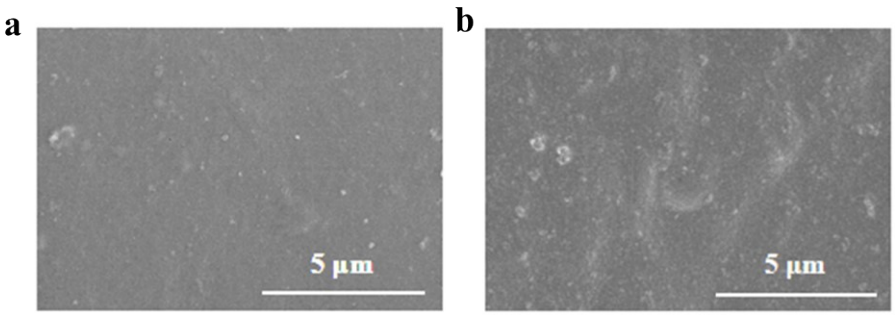

Figure S20. Surface SEM images of a) DETA-COF and b) TEPA-COF membrane.

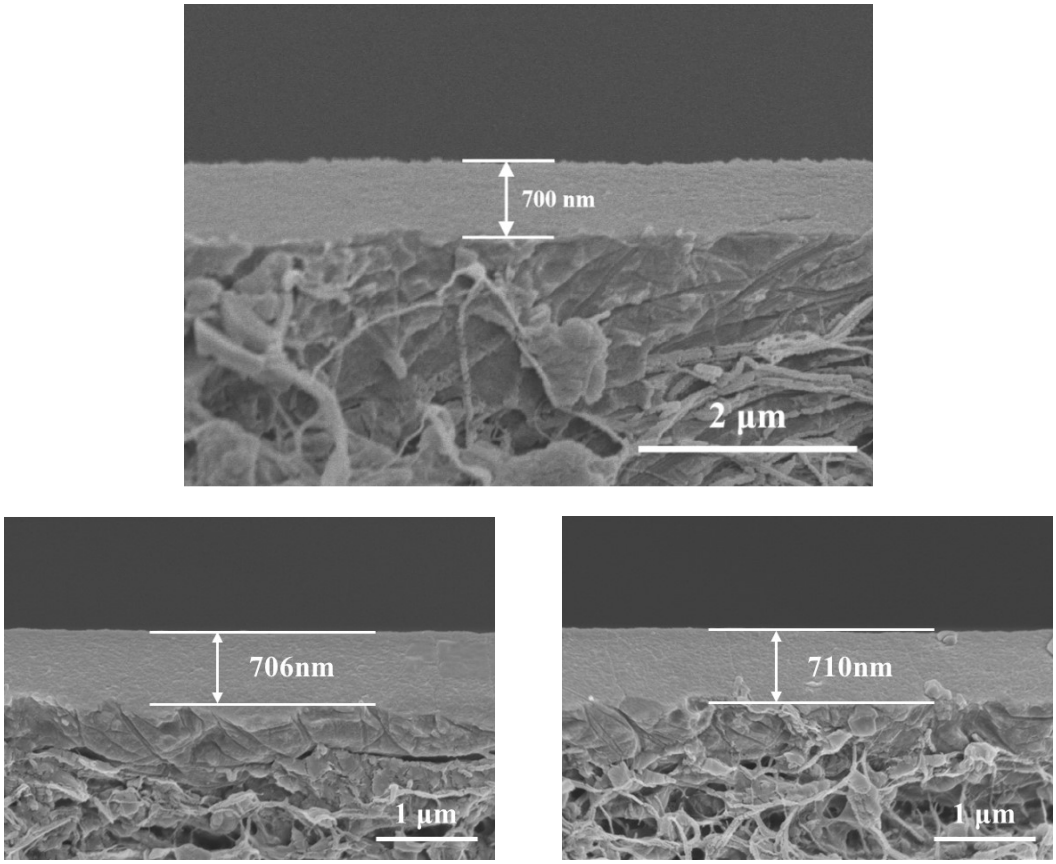

Figure S21. Cross-sectional SEM images of the TETA-COF, DETA-COF, and TEPA-COF membranes.

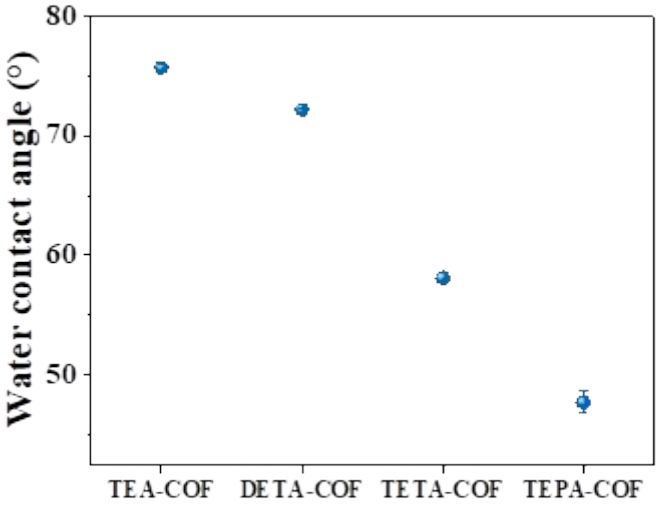

Figure S22. WCA test of TEA-COF, DETA-COF, TETA-COF, and TEPA-COF membrane.

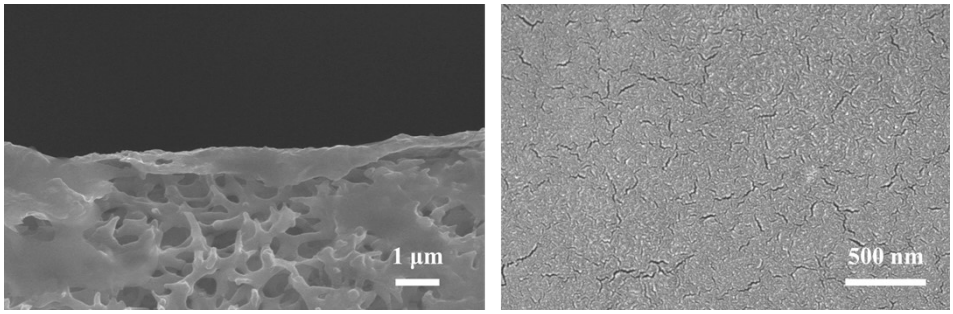

Figure S23. Surface and cross-sectional SEM images of pure COF membrane.

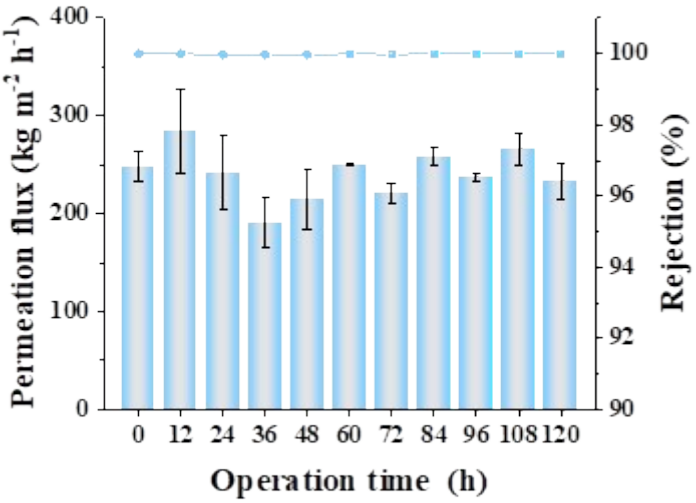

Figure S24. Long-term operational stability of TETA-COF membrane.

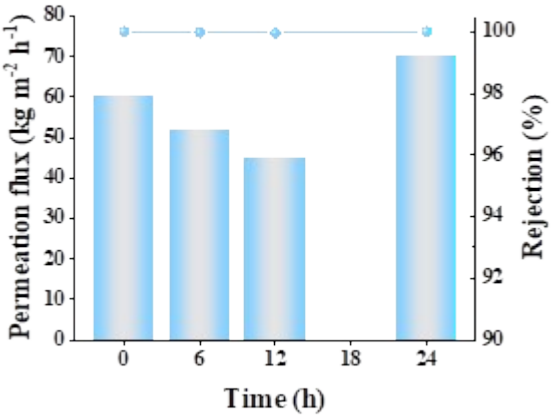

Figure S25. The desalination performance of the TETA-COF membrane when testing 3.5 wt% NaCl aqueous solution with 100 ppm NaClO.

Table S1. C/N ratio and addition contents analysis of DETA-COF, TETA-COF, and TEPA-COF nanosheets.

Sample	C/N ratio	Amine catalyst addition (%)
pure COF	6.00	0
DETA-COF	4.80	26.36
TETA-COF	5.20	27.32
TEPA-COF	4.85	26.24

Table S2. Summary of desalination performance of representative membranes reported in the literature.

Membranes	Desalination technique	Feed temperature (°C)	Water flux (kg m^{-2} h^{-1})	Salt rejection (%)	Ref.
POSS@GO	PV	80	112.7	99.98	[1]
PVA/PAN nanofiber composite	PV	55	~126.2	99.6	[2]
hydrophilic nanofibrous webs	PV	80	11	99	[3]
COF_{DT}-E18@cPVDF	VMD	55	~88.3	99.9	[4]
Graphdiyne	VMD	50	~130	99.9	[5]
Photothermal omniphobic membranes	VMD	30	2.94	>98	[6]
TETA-COF	PV	50	**230.1**	99.97	This work

P.S.: The membrane-based desalination technique includes pervaporation (PV) and vacuum membrane distillation (VMD).

References

(1) Zhan, X.; Gao, Z.; Ge, R.; Lu, J.; Li, J.; Wan, X. Rigid POSS intercalated graphene oxide membranes with hydrophilic/hydrophobic heterostructure for efficient pervaporation desalination. *Desalination,* 2022, **543**, 116106.
(2) Xue, Y. L.; Huang, J.; Lau, C. H.; Cao, B.; Li, P. Tailoring the molecular structure of crosslinked polymers for pervaporation desalination. *Nat. Commun.,* 2020, **11**, 1461.
(3) Yang, M.; Yao, N.; Li, X.; Yu, J.; Zhang, S.; Ding, B. Dual-Asymmetric Janus Membranes Based on Two-Dimensional Nanowebs with Superspreading Surface for High-Performance Desalination. *ACS Nano,* **2024**, *18* (48), 33159-33167.
(4) Zhao, S.; Jiang, C.; Fan, J.; Hong, S.; Mei, P.; Yao, R.; Liu, Y.; Zhang, S.; Li, H.; Zhang, H. *Nat. Mater.,* 2021, **20**, 1551-1558.
(5) Chen, H.; Liu, X.; Gong, D.; Zhu, C.; Liu, G.; Fan, J.; Wu, P.; Li, Z.; Pan, Y.; Shi, G. *Nat. Water.,* 2023, **9**, 800-807.
(6) Asadolahi, M.; Fashandi, H.; Ghodsi. *Chem. Eng. J.,* 2024, **500**, 157428.